

A Multibandwidth Probing Method for Tissue Scattering Microstructure Characterization.

N.A.H.K. Rao¹, M. Helguera^{1,2}

¹ Center for Imaging Science
Rochester Institute of Technology
Rochester, NY, 14623

² CENIDET, Cuernavaca, México

Abstract- In medical ultrasound the normalized second intensity moments of the echo signal can depend on the imaging system resolution cell volume (axial and lateral resolution) in addition to the scattering microstructure. We propose a multibandwidth probing technique in an attempt to separate the two. Theoretical relationships between second intensity moments, (scattering coefficients, scatterer spacing, and its randomness) and the system's cell volume are established. Experiments on water filled sponge structures with pore size varying from .5mm to 2mm and pig liver tissue are performed. The slope and intercept values from normalized second intensity moments versus (cell volume)⁻¹ graph are shown to be of diagnostic value in structure characterization.

INTRODUCTION

Recently, there has been a renewed interest at understanding the relationship between the different moments of the ultrasound echo signal and the scattering microstructures. In the non-Rayleigh regime [1, 2], where deviations from fully developed speckle exist, the intensity moments estimated from the echo signal depend on several factors: (1) the number density of the scatterers in the medium and the resolution cell volume of the imaging system, more importantly, the product of the two [3], that is, the number of scatterers in the resolution cell, (2) the statistical distribution of the scattering cross-sections which themselves may show a frequency dependence [5], (3) the presence of any subresolution (unresolved) periodic or nearly periodic structure in the sonicated medium and its relationship to the dominant frequency in the interrogation pulse. [6].

The purpose of this paper is to experimentally examine the effect of all the factors mentioned above on the echo signal analysis. Our first task is to understand how the estimated normalized second intensity moment depends on the resolution cell volume, and devise a method to remove its influence. Only then can the moments

be considered to depend on the scattering microstructure alone. In our experiments we probe the microstructure with several pulses of different bandwidths but same center frequency f_0 and examine the behavior of the second intensity moment as a function of bandwidth. In a previous paper [7] we presented in detail the theoretical foundation of our work based on Jakeman's analysis [8] of the non-Gaussian behavior of scattered waves. The normalized second intensity moment is derived by applying random walk concepts under narrow bandwidth assumptions. To confirm our theory, we performed simulations of the effect of scattering as well as diffraction over the range of bandwidths utilized in our experiments. We noted that the diffraction term acts as a low pass filter with a large bandwidth, i.e. it varies slowly over the small bandwidth of the drive signal, and its main effect is on the amplitude of the incident pulse. On the other hand, the scattering term acts as a high pass filter whose effect is negligible on the incident pulse under the narrow bandwidth regime. With these considerations, the echo signal from each scatterer becomes a slightly bandpass filtered, but mostly amplitude weighted, and time shifted version of the drive signal. The resultant signal can be written as a phasor sum:

$$s(t) = e^{j2\pi f_0 t} \sum_{n=1}^M E_n e^{j\phi_n} \quad (1)$$

where M is the number of scatterers in a volume V_T that is formed by considering say, a cylinder of diameter equal to 20 dB beam width and length equal to 20 dB pulse width.

$E_n = a_n B(r_n, z) A(t - t_n)$, where a_n is the backscatter coefficient at the dominant frequency f_0 , $B(r_n, z)$ is the transducer beam profile value at the scatterer location, $A(t - t_n)$ corresponds to the pulse envelope and $\phi_n = -2\pi f_0 t_n$.

The second normalized moment [7,8] of the intensity distribution $I(t) = |s(t)|^2$ can be written as

$$\frac{\langle I^2 \rangle}{\langle I \rangle^2} = 2 + \frac{\langle a^4 \rangle}{\langle a^2 \rangle^2} \frac{1}{\langle N \rangle V_e} = 2 + \text{slope} \cdot \frac{1}{V_e} \quad (2)$$

where $\langle N \rangle = \langle M \rangle / V_T$ and V_e is given by

$$V_e = \frac{c \left[\int \int 2\pi r dr B^2(r) \int A^2(t) dt \right]^2}{2 \left[\int \int 2\pi r dr B^4(r) \int A^4(t) dt \right]} \quad (3)$$

c is the speed of sound. V_e can be calculated from the experimental intensity point spread function (PSF) of the imaging system. We will call it the "resolution cell volume". When we vary Δf we also affect $A(t)$, the pulse envelope. This in turn affects the V_e term in Eq. 3.

V_e is the only variable in Eq. 2 that is system dependent and will be exploited for the estimation of tissue structure term we call "slope".

If the cell volume is too large ($V_e \rightarrow \infty$), the estimate $\langle I^2 \rangle / \langle I \rangle^2$ approaches its Rayleigh limiting value of 2 (fully developed speckle). However, if there is a dominant constant phasor term present in the random walk sum (Eq. 1) then this limiting value can be lower than 2 [6,7]. This can take place due to constructive interference from an almost periodic structure with spacing equal to an integer multiple of the dominant wavelength $\lambda = c/f_0$. We believe we are observing this phenomenon in most of the scattering structures that we have studied, including pig liver.

EXPERIMENTAL METHODS

We recorded the echo signals from two sponge structures immersed in water and fresh pig liver tissue. Care was taken that no air bubbles were trapped in the sponges. One sponge, labeled Sample 1, had large mean pore size of about $d=2\text{mm}$ (similar to the lobular structure of the liver). The other sponge had mean pore size of about $d=.5\text{mm}$.

The 13mm diameter circular disk 3.5MHz medium focused transducer had a focal length of 4.5cm. The sponge surface as well as the liver surface were positioned at the focal length of the transducer and held perpendicular to the beam axis. The transducer was excited with programmable signals generated by a waveform generator (Analogic Corp. Model 2020) as:

$$p(t) = .5 \left[1 - \cos\left(\frac{2\pi t}{T}\right) \right] \cos(2\pi f_0 t); 0 \leq t \leq T \quad (4)$$

where $A(t)$ corresponds to a Hanning function envelope. f_0 was fixed at 3.5 MHz, the center frequency of the transducer. By varying T , the width of the envelope, the bandwidth Δf of the pulse was varied from .2MHz to 1MHz in steps of .2MHz approximately. 10 μs of echo signal, centered in the focal zone were recorded in each case at a sampling interval of .04 μs with an 8 bit digitizer (Analogic Corp. DATA 6500). For every bandwidth, from each sponge, and the liver tissue, echo signals were recorded at 30 different locations, obtained by translating the transducer in the plane perpendicular to the beam axis with a stepper motor, covering a 10mm by 3mm area. Each translation was 1mm.

The two dimensional PSF was measured in a separate experiment by placing and scanning a .25mm nylon wire at the focal zone of the transducer.

Similar experiments were performed with samples held at 6 cm from the transducer. This we refer to as the far field (ff). Separate PSF measurements were also performed at this distance.

The intensity signal $I(t)$ is the square of the envelope detected echo signal $s(t)$. Both time and ensemble average (over 30 lines) were combined for estimation of $\langle I \rangle$ and $\langle I^2 \rangle$

RESULTS AND ANALYSIS

Fig. 1 shows the plot of the normalized second intensity moments, i.e., $\langle I^2 \rangle / \langle I \rangle^2$ (referred to as Iratio), as a function of the interrogating pulse bandwidth Δf in the focal zone, for the two different sponge structures and the pig liver tissue measured at two different orientations. Fig. 2 shows the plot of the normalized second intensity moment as a function of bandwidth Δf in the far field for the two sponge structures. Standard deviation was about 15% of the Iratio values. From the figures one can appreciate that the normalized moments increase approximately linearly with Δf . And that the slope is higher for the large pore size sponge, sample 1, and the liver tissue than for the small pore size sponge (sample 2).

To remove system effects, the resolution cell volume, V_e was calculated from the PSF measurements at different bandwidths and the two different depths. (focal zone and far field). As a simple approximation, this volume can be regarded as a cylindrical space bounded by a circle of diameter equal to 6dB beamwidth $B(r)$ and the height equal to $c/2$ times the 6dB pulse width of $A(t)$. In this paper we have used this approximation, but also included the volume due to sidelobe structure surrounding the main lobe. It

should be pointed out that V_e as defined in Eq. 3 is the corrected effective volume since it is an average, weighted by the PSF value at different points in the cell space. Calculation of V_e as defined in Eq. 3 from the PSF is under investigation.

Once the V_e are estimated for each Δf from the PSF, we get a calibration curve shown in Fig. 3. This is then used as a lookup table to replot the data in Figs. 1 and 2 as a function of $1/V_e$. (See Figs. 4 and 5).

A linear regression on lowest bandwidth points was performed and "slope" and "intercept" estimates were obtained for each sponge and liver tissue samples. The slope values for small and large pore sponge were 12.09 and 36.28 respectively, and intercepts were 1.25 and 1.73 respectively. For the liver sample the slope was 50.2 and intercept 1.18. The histologic section of liver clearly had lobular structure that was closer to the structure of the large pore sponge than the small one. The slope data confirm this quantitatively. In the far field the slope and intercept values for the large pore sponge were 39.5 and 0.96, and 12.52 and 1.29 for small pore. While the slope values are not different in the two zones, the intercept seems to change.

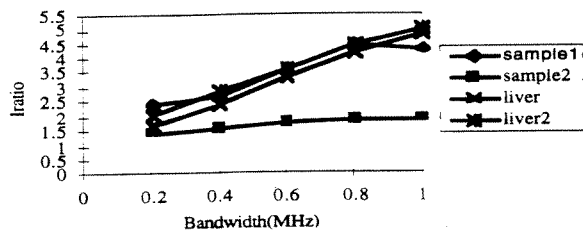


Fig. 1. $\langle I^2 \rangle / \langle I \rangle^2$ (Iratio) as a function of bandwidth. Focal zone.

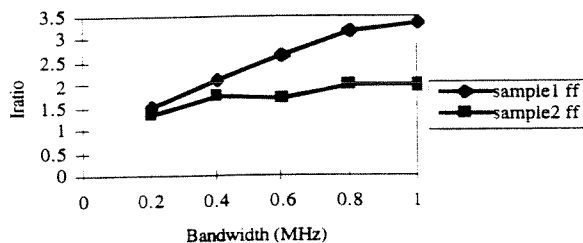


Fig. 2. $\langle I^2 \rangle / \langle I \rangle^2$ (Iratio) as a function of bandwidth. Far field.

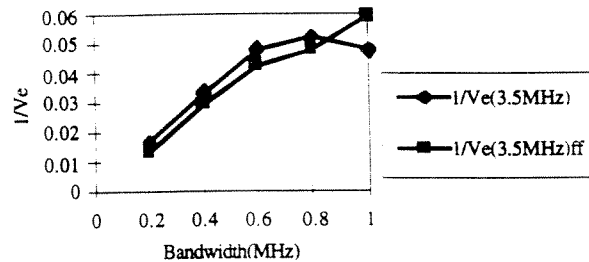


Fig. 3. Inverse of resolution cell volume as a function of bandwidth. \diamond - Focal zone and \blacksquare - far field.

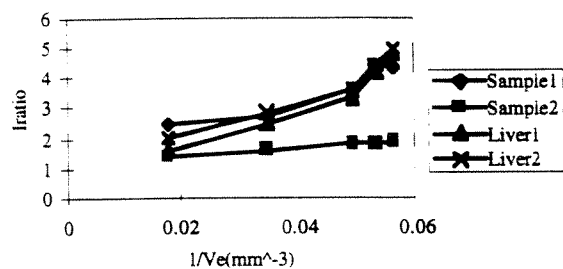


Fig. 4. $\langle I^2 \rangle / \langle I \rangle^2$ (Iratio) as a function of cell volume. Focal zone.

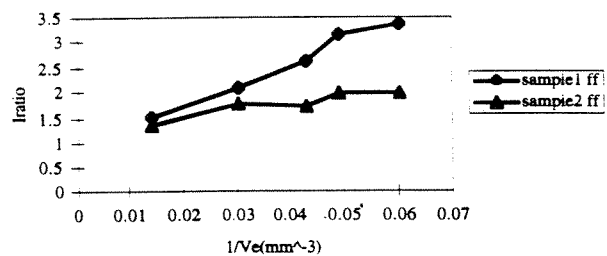


Fig. 5. $\langle I^2 \rangle / \langle I \rangle^2$ (Iratio) as a function of cell volume. Far field.

DISCUSSION

The intercept of the curves in Figs. 4 and 5 correspond to the Rayleigh limit case, in the sense that the number of phasors significantly contributing to the phasor sum in the random walk problem becomes large. However, this

behavior is also governed by the phase distribution of the phasors, ϕ_n . If these phases are independent and their probability distribution is uniform, then the expected value for the normalized intensity moments is 2. If there is spatial correlation due to underlying periodicity in the scattering structure, the limiting value can be lower than 2 [7]. This is manifest due to the constructive interference and coherent buildup of a constant phasor term. We believe this is the explanation for the low values for the intercepts.

According to Eq. 2, the slope estimate should be inversely proportional to $\langle N \rangle$, the scatterer number density. Our quantitative estimates reflect this behavior if we assume that the individual strands in the sponge or the lobular boundaries act as scatterers. Large pore sponge and the liver tissue have higher slopes followed by small pore sponge. However, it is noteworthy that the slope value also depends on the scattering medium via the term $\langle a^4 \rangle / \langle a^2 \rangle^2$. We cannot separate this term from $\langle N \rangle$. The combined term is also sometimes referred to as the "effective scatterer number density" [5]. Furthermore, the slopes don't change significantly as the cell volume is increased in the far field indicating that system PSF effects have been removed properly.

CONCLUSIONS

The method described in this paper performs the estimation of two features: the slope and the intercept, from a series of low bandwidth probing of the microstructure. These feature values convey different information about the microstructure. The slope depends on the "effective scatterer number density" and the intercept mostly depends on the regularity of the structure. These parameters have been estimated over a small volume on the order of 10mm x 2mm x 8mm.

Chen et. al. [5] have proposed a method to estimate the effective scatterer number density at different frequencies by calculating the statistical moments on the Fourier transform of the echo signal. We believe that the inverse of our low bandwidth slope estimate represents a similar scatterer number density at the dominant frequency f_0 . However, in our method, as we track the low bandwidth behavior (as $\Delta f \rightarrow 0$), we obtain an intercept value, which may prove to be of value in structure characterization.

Acknowledgment- This work was supported in part by a grant from NIH, CA 71004-01.

REFERENCES

- [1] J.F. Chen, et. al. "Non-Gaussian versus non-Rayleigh statistical properties of ultrasound echo signals", *IEEE Trans. Ultrason. Ferro. Freq. Cont.* **41**, 435-440 (1994).
- [2] V.M. Narayanan, et. al. "Non-Rayleigh statistics of ultrasonic backscattered signals", *IEEE Trans. Ultrason. Ferro. Freq. Cont.*, **41**, 845-852 (1994).
- [3] N.A.H.K Rao, H. Zhu "Simulation study of changes in ultrasound speckle statistics with the system point spread function", *J. Acoust. Soc. Am.* **95**, 1161-1164 (1994).
- [4] G.E. Sleepe, P.P. Lele "On estimating the number density of random scatterers from backscattered acoustical signals", *Ultr. Med. Biol.* **14**, 709-727 (1988).
- [5] J.F. Chen, et. al. "Statistical uncertainties in estimates of an effective scatterer number density for ultrasound", *J. Acoust. Soc. Am.* **96**, 2556-2563 (1994).
- [6] N.A.H.K. Rao, M. Aubry "Evaluation of a pulse coding technique for spatial structure characterization", *IEEE Trans. Ultrason. Ferro. Freq. Cont.* **41**, 660-663 (1994).
- [7] N.A.H.K. Rao et. al. "On understanding the relationship between ultrasound speckle and the scattering microstructure" in *Acoustical Imaging*, **26**, Plenum Press (1997).
- [8] E. Jakeman, R.J.A. Jough "Non-Gaussian models for the statistics of scattered waves" *Advances Phy.* **37**, 471-529 (1988).